Solar Energy Materials & Solar Cells 292 (2025) 113801

Contents lists available at ScienceDirect

Solar Energy Materials and Solar Cells

journal homepage: www.elsevier.com/locate/solmat

Development of low-cost, light weight c-Si photovoltaic modules with potential for applications in VIPV

Bartlomiej Fligier [a], Srinath Nalluri [b], Bernard Moćko [b], Kazimierz Drabczyk [c,d], Grażyna Kulesza-Matlak [c], Katarzyna Jajczak [a], Pradeep Padhamnath [a,*]

[a] AGH University of Krakow, Krakow, Poland
[b] Solar Energy Research Institute of Singapore, National University of Singapore, Singapore
[c] Institute of Metallurgy and Material Science, Polish Academy of Sciences, Krakow, Poland
[d] University of Bielsko-Biala, Bielsko-Biala, Poland

A B S T R A C T

Vehicle integrated photovoltaics (VIPV) is gathering attention by researchers and industry alike to help in decarbonization of transport industry. While PV panels have been integrated to the vehicles to support auxiliary functions, their wide scale implementation is limited by their size, weight and rigidity. In this work we present a proof-of-concept method to produce bi-facial PV panels with fibre-glass reinforced composite fabric (GRCF) using vacuum resin infusion process. These modules are specifically designed for integrating with an electric car and to be used as a power source to charge the batteries. Mini modules are fabricated using two interdigitated back contact solar cells sandwiched between layers of GRCF sheets. The modules are prepared by drawing the resin under a suitable vacuum through the different GRCF layers and allowing the resin to cure at room temperature. The modules are prepared at room temperature without using a stringer or laminator. Three different metal end-strips are used to assess their performance in the finally prepared module. The modules are subjected to the damp-heat test to analyse the degradation in the modules and the suitability of the fabrication process. Results show that resistance losses and optical losses play a vital role in the final losses resulting from degradation of the modules. Finally, we have shown in this work that it is possible to fabricate such modules using low-cost technology. By fine tuning and scaling-up the process, it is possible to produce modules of any size which could further help in the rapid integration of c-Si PV modules in vehicles.

1. Introduction

Vehicle Integrated Photovoltaics (VIPV) could be seen at the next technological advancement in the field of pollution free electrical vehicles. VIPV broadly refers to the integration of the PV panels on various surfaces of the vehicles. The integrated PV system can generate electricity while the vehicle is exposed to sunlight, whether stationary or moving. Use of such VIPV systems have been studied for powering auxiliary systems such as air-conditioning and refrigerator [1,2], to charge service batteries in emergency vehicles [3] and buses and trucks used for public and goods transport respectively [4–6]. Recent studies have shown excellent potential for such VIPV systems [7,8]. Several automobile producers have been developing such VIPV technologies and showcasing them in concept vehicles [9]. Application of VIPV is largely supported by the increase in the energy generation per unit weight of PV modules, at lower incremental costs [7]. Despite these opportunities, development and integration of lightweight low-cost PV modules in commercial vehicles remains a challenge [10,11].

To decrease the weight of the PV modules, researchers have used glass fibres as encapsulants and backsheet in PV panels making the panels lighter[10–12]. Recently, the use of glass-fibres reinforced composites fabric (GRCF) was suggested to be used as front sheet in the PV modules [13]. GRCFs modules are lightweight, more flexible than glass modules and have excellent mechanical and chemical stability [12–17]. Additives for UV resistivity when added to resin, result in some initial loss in short circuit current density (J_{sc}), however, further drop in J_{sc} on exposure to UV light is lower than in the modules without the UV additives [18,19]. Despite these advances in the incorporation of the GRCFs in PV panels, such panels are limited by their transmittance properties [12,13,15,17–22]. Vacuum infusion process has recently gathered attention as an alternative, low-cost process to fabricate solar PV modules with glass-fibre composites materials [18,19,21,22]. In the recent study, a glass fibre reinforced plate was used on the rear side of the monofacial modules while a combination of GRCF and polymers were used on the front side [13] with the use of a vacuum infusion process and laminator. The lamination temperature was 140 °C while

This article is part of a special issue entitled: MIW2024 proceedings published in Solar Energy Materials and Solar Cells.

* Corresponding author.
E-mail address: ppadhamnath@agh.edu.pl (P. Padhamnath).

https://doi.org/10.1016/j.solmat.2025.113801
Received 30 January 2025; Received in revised form 17 June 2025; Accepted 18 June 2025
Available online 21 June 2025

800 mbar of pressure was applied for 30 min.

In this work we present proof-of-concept bifacial modules using GRCF as both front and the rear side of the PV panels. These panels are intended to be integrated to custom built solar-powered car (Fig. 1) and solar powered boat for participating in various competitions worldwide. While other applications of the developed modules are possible (Fig. 2), the work presented here is focussed more on the development of the module fabrication process rather on the applications of the modules. We present the development of the module fabrication set-up and a process to prepare the modules without the laminator. The front and rear layers were optimized for transmissivity and mechanical strength. The modules were fabricated with interdigitated back contact solar cells procured commercially. We use different materials as external connectors to see the impact of the environmental factors on the degradation of the modules. For the intended application of the modules in solar powered cars and boats, several mechanical tests are required, which could not be performed at this stage. Hence, we do not claim the modules to be ready for integration into the vehicles. The aim of this work is to expose the modules to accelerated degradation tests (damp heat) tests and try to understand the robustness of the fabricated process and the power loss resulting from exposure of the modules to moisture and heat.

2. Experimental details

The bifacial PV modules were fabricated in a laboratory without clean room environment. All the equipment used for fabricating the modules were self-designed and assembled in the laboratory.

2.1. Module lamination platform

The module layup and lamination with the help of resin was performed on a heated platform. The platform was fabricated on a flat layer of borosilicate glass used for high temperature applications. Borosilicate glass was chosen as the surface due to its ability to withstand both spatial and temporal temperature gradients, and sufficient mechanical strength. Two heating plates, each similar the size of a single 5-inch solar cell (130mmx130mm), were attached to the back of the glass. Each heating plate was connected to a temperature controller with feedback, allowing for individual control of each plate's temperature. The heaters were installed to maintain similar temperatures during repeated process runs, to help the resin flow, and to maintain a similar curing temperature, as the environment in the laboratory was not controlled. An earthing connection was taken from the centre of the platform through a leakage current detector to avoid any accidental leakage current. The set-up was connected to the main power supply with the help of variable current controller (1–15 A). The entire setup was placed on an insulated medium density fibreboard (MDF) for thermal and electrical insulation. Fig. 3 shows the prepared module lamination platform on the MDF.

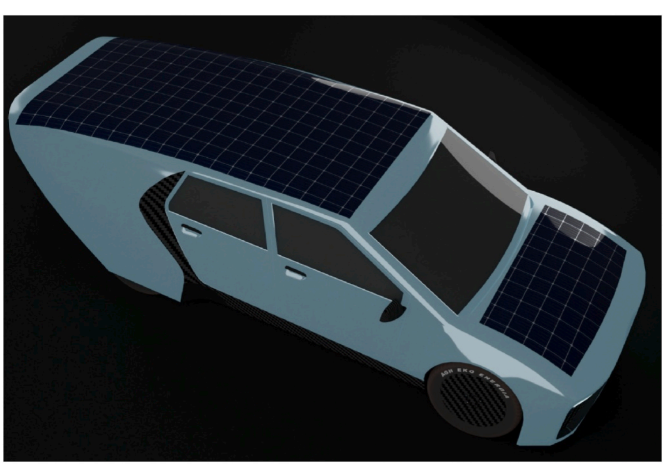

Fig. 1. A rendered image of the electric car showing the integrated modules designed in this work. This car is designed for an endurance race across long distances and can carry up to four people and supplies.

2.2. Vacuum pump system for degassing and impregnation of the resin

The impregnation of the thermosetting resin through the module is abetted by the vacuum. Further, it was necessary to degas the resin as much as possible before the process to prevent formation of bubbles inside the modules. For these purposes a vacuum chamber and flow system were designed. The vacuum pump system comprised of a vane pump capable of reaching a vacuum of −1 Bar (−100 kPa, relative to the atmospheric pressure), an intermediate resin collection chamber to control the magnitude and the direction of vacuum and to prevent any ingress of resin into the pump, and a degassing chamber for the pretreatment of the resin. The pump was connected through a bidirectional control valve to the resin collection chamber. The module laminating platform was connected to the vacuum pump through an extension in the resin collection chamber. The degassing chamber was connected to the resin collection chamber through another bidirectional control valve. The control valves were manually operated to control the vacuum applied to the degassing chamber and to the module lamination platform through the resin collection chamber. Vacuum gauges were installed on the common line connecting the degassing chamber and the resin collection chamber. Fig. 4 shows the vacuum system with different components labelled for clarity.

2.3. Module fabrication process

Commercially procured 127mmx127mm Interdigitated back contact (IBC) solar cells were used to fabricate the minimodules used in this work. According to the specifications provided by the supplier, the solar cells had an open circuit voltage (V_{oc}) of 713 mV, short circuit current (I_{sc}) of 5.79 A and a fill factor of 81.35 %. The maximum power output (P_{max}) of each solar cells was rated at 3.35 W. Two such solar cells joined in series were used to fabricate a mini-module module. The solar cells were interconnected using specially designed tin-plated copper interconnection strips supplied with the solar cells. A manual soldering device with lead free solder paste (Sn-Ag-Cu) was used to interconnect the solar cells, at temperatures between 220 and 230 °C. Fig. 5 shows the interconnected solar cells. Two end leads were attached to the two ends of the interconnected solar cells. The ends of the leads were covered with tape to prevent interaction with resin during the resin impregnation and lamination process. Three different end-strips were provided by our industry partner which were made from Al alloy, weather resistant Cu alloy and a Ni alloy for electrical applications. The Cu and Ni alloy were specially developed by the industry partner and details about their composition are proprietary information. The cross-sectional area in terms of thickness (t) and width (w), and resistivity values of the different metal strips are mentioned in Table 1.

The values of coefficient of thermal expansion (α) and resistivity (ρ_{given}) were provided by the supplier. Additionally, the value of the resistivity was also calculated (ρ_{calc}) in our laboratory. For the purpose of measuring resistivity, the strips were cut in lengths of 200 mm, and resistance between the two ends was measured with a standard resistance meter. Later the resistivity was calculated according to the formula, $\rho = R^*A/l$, where ρ is the resistivity in Ω-m, A is the cross-section area in m^2 and l is the length of the strip in meters. The cross-sectional dimensions of the metallic strips were measured using a thickness micrometre. Five measurements were taken for each dimension at different points along the strips.

Frekote release agent was applied to the glass surface to allow for the easy removal of the modules after fabrication. The corners of the glass plate were covered with paper tape to prevent the application of release agent. This was done to provide good adhesion between the glass plate and the butyl tape which was used later to secure the different layers of

Fig. 2. Artistic images (rendered) of possible applications of the flexible bifacial modules presented in this work within the university campus.

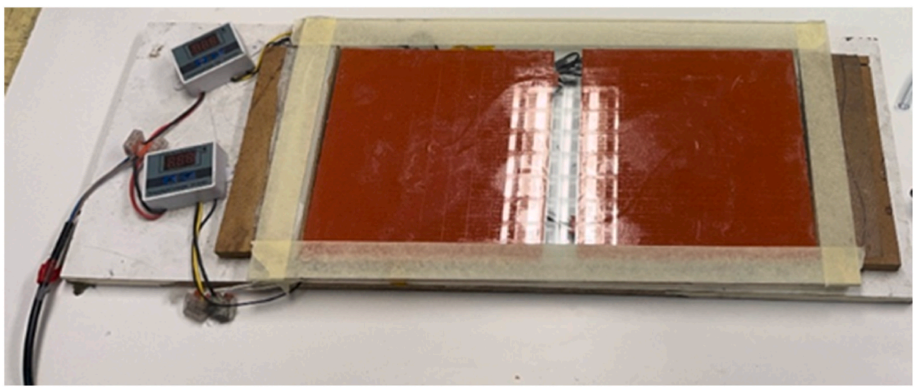

Figure-3. The module lamination platform using borosilicate glass with integrated heating plates and temperature controllers. The work area is defined by the insulated tape at the boundaries.

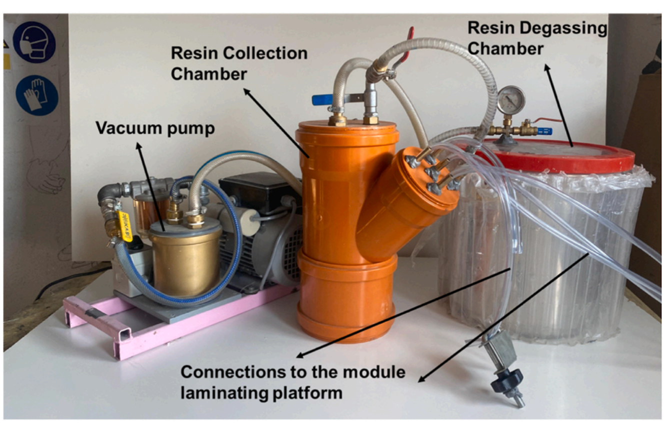

Fig. 4. Vacuum system comprising the vacuum pump, the resin collection chamber and the resin degassing chamber.

the module during processing. The different layers of materials used for preparing the modules were cut according to the size and dried in a hot air oven at 60 °C for 30 min. A layer fibreglass chopped strand mat (150 g/m^2) and a layer of fibreglass reinforced composite fabric (GRCF) (50 g/m^2) was used on the front, while another layer of twill-weave fiberglass reinforced composite fabric (TW-GRCF) (250 g/m^2) was used for the rear surfaces. Fig. 6 shows the cross-section schematic of the modules presented in this work. Another layer Compoflex® SB150 (Fibertex Nonwovens) release film was used on both sides of the module to facilitate easy removal of the module. This film acts as a barrier between the module and glass surface on the rear side and the vacuum bag on the front side and prevents the module from bonding with the either surface. This film is not a part of the module. The release film, if removed carefully, could be reused. Furthermore, the release film leaves behind a porous surface on the rear side of the module, which makes the module easier to adhere to a vehicle's bodywork.

Cuts were made in two sets of PPE tubes for a measured length (≈130 mm) at allow for the entry of resin and for evacuation of air to induce vacuum assisted flow of the resin. Tubes for evacuating air and for the introduction of the resin were next attached to the alternate end of the modules with the help of butyl tape. On one end, the tube was connected to the vacuum pump, while on the other end was left free for introducing the resin. Finally, the vacuum bag was attached on the top with the help of butyl tape and the air was evacuated by switching on the vacuum pump for 20 min. The vacuum pump was switched off and any air ingress was measured for a period of 10 min with the help of the vacuum gauge. If the pressure held steady, it meant that a good seal was achieved, and the setup was ready for infusion. Fig. 7 shows the lamination platform after the vacuum bag was sealed with the module to be fabricated.

Epoxy resin (LG 700) was mixed with the hardener (HG 700) were mixed in the ratio 100:30 and kept inside the degassing chamber until all the formation of the bubbles ceased. At this point the resin mixture was assumed to be sufficiently deaerated. Concurrently, the heaters were switched on and the temperature controllers were set at a temperature of 60 °C. After the temperature was steady, the resin infusion was started by switching on the vacuum pump and introducing the resin from the

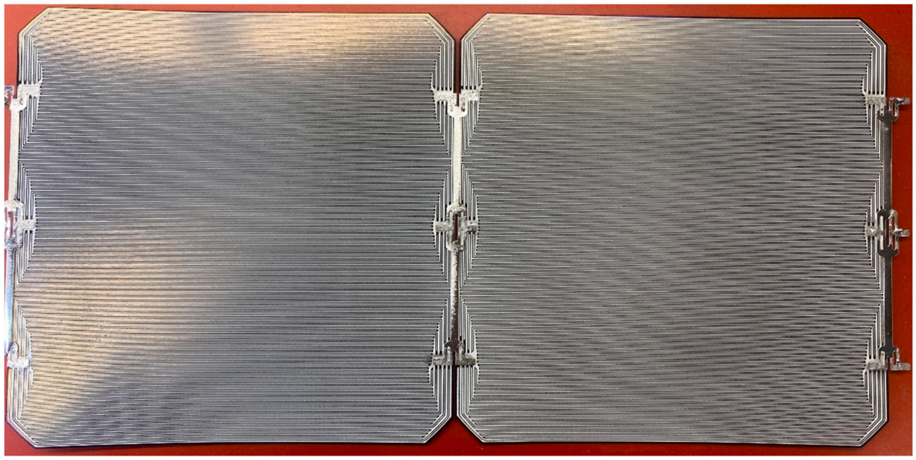

Fig. 5. Interconnected IBC solar cells. The interconnection was done manually using a hand-held solder device, with lead free solder paste.

Table 1
Cross section area and electrical resistivity of the metal strips used as end strips for modules fabricated in this work. The dimensions of the cross-section area were measured using thickness micrometre.

Sr no	Material	Cross section area (t*w) mm^2	α [10^{-6} °C^{-1}]	ρ_{given} [x10^{-9} Ω-m] (at 25 °C)	ρ_{calc} [x10^{-9} Ω-m] (20–25 °C)
1	Al alloy	0.5*2 ± 0.13	23	27.3	28.2 ± 1.3
2	Cu alloy	0.2*5 ± 0.11	17	17.4	17.2 ± 1.1
3	Ni alloy	0.1*4 ± 0.11	12	55	59.9 ± 2.1

tube on the opposite side. The resin is allowed to impregnate throughout the module. Once the resin starts appearing on the other side of the tube, the heaters are switched off, the vacuum pump is closed, and the tubes are crimped and sealed. The modules were allowed to cure overnight at room temperature (≈8–10 h), after which the vacuum bag and the release film on the modules were removed. The final module obtained after curing is shown in Fig. 8. Nine such modules were exposed to DHT in total, three with each type of metal end strip. In Fig. 8, the part of the module above the solar cells appears more transparent than the surrounding additional GRCF stack (highlighted region). This is due to the dense TW-GRCF used at the rear is less transparent than the layers used at the front.

2.4. Characterization details

The optical characteristics of the prepared laminates were measured using the UV–VIS spectrometer (Agilent Technologies). The simulated current voltage characteristics of the prepared modules were tested using Pasan High light lab PV simulator. The modules were measured in two-point configuration. The ageing performance and moisture ingress in the modules were analysed by subjecting the modules to Damp-heat test (DHT) in the Thermotron 3300 Lab test chamber. The damp hear test was carried out at 85 °C and 85 % relative humidity. Measurements were done after 72 h, 144 h and 300 h, 600 h and 1000 h of exposure. The Electroluminescence (EL) Images of the modules were measured using a custom designed EL set-up with a modified Nikon D610 DSLR camera to capture infrared wavelengths.

3. Results and discussion

3.1. Optical characterization and optimization of the GRCF stack

The first step in the fabrication process was deciding the optical stack to be used for making the modules. To finalize the GRCF stack for the modules optical and mechanical characterization of the stack (without the solar cells) was done. The different combination of materials tested for preparing the GRCF stack and their weight in grams per m^2 are given in Table 2. The first layer from the front side was layer of GRCF with different area specific weights as shown in Table 2. The second layer was the fibreglass chopped strand mat which was kept unchanged for all samples. The last layer (or the rear-side layer) was TW-GRCF with different area specific weights as mentioned in Table 2. The GRCF stacks

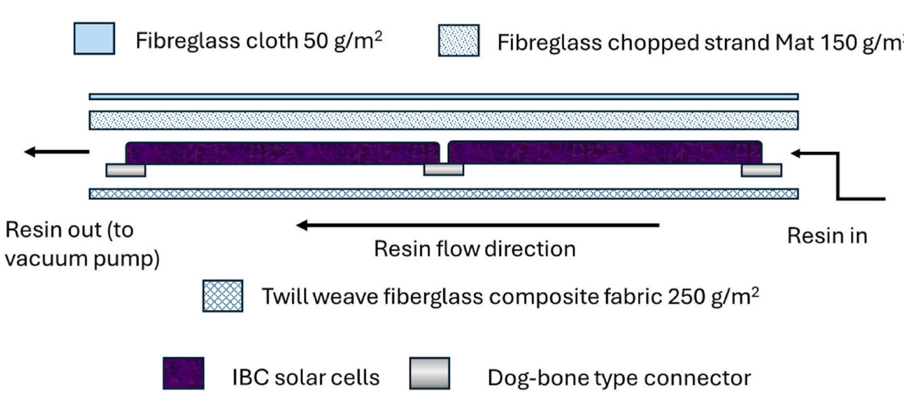

Fig. 6. Schematic of the cross section of the GRCF modules fabricated in this work using IBC solar cells. The cross section shows the different layers incorporated into the module, the resin entry and exit points and the direction of flow of the resin.(image not drawn to scale).

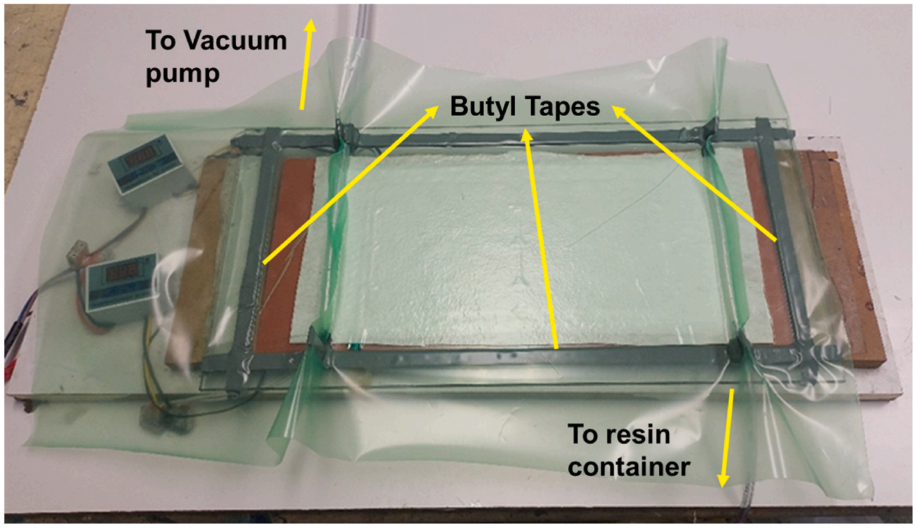

Fig. 7. The module lamination platform with the interconnected solar cells, different composite layers and the vacuum bag. The pipes for introduction of vacuum and resin are also shown and marked accordingly. At this stage, the bag is firmly attached to the platform with the help of butyl tapes and sealed by evacuating the air with the help of vacuum pump.

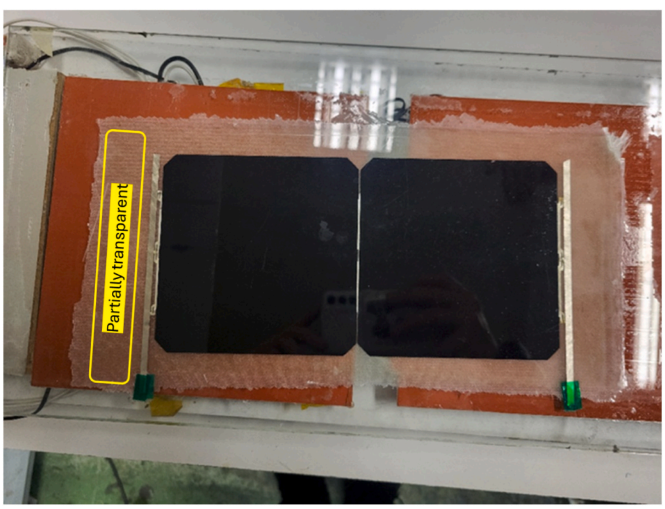

Fig. 8. Finished module after resin impregnation and curing, and removal of the vacuum bag and the release film on both sides. The GRCF stack extending on the sides (highlighted region) is visibly less transparent than the layers on top of the solar cells.

Table 2
The different GRCF stacks used for transmittance characterization using UV–VIS spectrometer. The different stack components are identified by their weight in g/m^2. The thickness of the different layers and the weight of the different stacks have also been added.

Stack#	Front layer-1 [g/m^2]	Front layer-2 [g/m^2]	Rear layer [g/m^2]	Thickness [mm]	Weight [g]
S1	50	150	150	1.02 ± 0.03	3.55 ± 0.02
S2	50	150	250	1.12 ± 0.05	3.90 ± 0.02
S3	50	150	450	1.35 ± 0.02	4.21 ± 0.03
S4	150	150	250	1.28 ± 0.02	4.15 ± 0.03
S5	150	150	450	1.42 ± 0.03	6.01 ± 0.03

were prepared using the process similar to that followed for preparing modules (resin infusion), without incorporating the solar cells and later cut into smaller samples of 50 mm × 30 mm size. Each stack is represented by the code S#. A standard PV glass (3.2 mm thick, 7200 g/m^2] was also used as a reference. The cross section of the GRCF stack prepares as optical test samples is shown in Fig. 9.

The transmittance of the cured GRCF stacks as measured using UV–VIS spectrometer is shown in Fig. 10. It was observed that the transmittance was higher for all the stacks with 50 g/m^2 GRCF. The best transmittance was observed for the lightest layer, with 50 g/m^2 GRCF at the front and 150 g/m^2 TW-GRCF at the rear. However, while fabricating modules with this layer, it was observed that the solar cells cracked when the module was being recovered from the platform and the release film was being peeled off. Hence, the stack with next best values of transmittance (S2) was used for fabricating a test module. In this case, it was observed that the solar cells were not damaged after the release film was peeled off. Both S1 and S2 exhibited similar transmittance throughout the entire range of wavelengths, however, S1 performed slightly better than S2 in the wavelength range of 300–400 nm and further in the infra-red range, which could be beneficial for bifacial modules. Further development of a gentler peeling process, or automation of the peeling process could enable the use of the light-weight GRCF stacks for fabricating the modules.

3.2. Damp heat test of the fabricated modules

The modules were characterized after fabrication and before introducing them to the damp heat chamber. Table 3 shows the values obtained from I-V measurements (two-point configuration) of the modules before the damp heat tests. The module type is referred to the material of the end strip used in the module. For comparison, the solar cell characteristics as provided by the supplier are also mentioned. It was observed that while both I_{sc} and V_{oc} were preserved, and the FF deteriorated from the cell to module. The FF loss could be correlated to the series resistances and to the imperfect manual soldering process. As expected, the modules with Ni-alloy end strips resulted in highest series resistance (R_s) and, consequently lowest FF among the three types of modules. Furthermore, the modules were measured in two-point configuration which could have contributed to the slightly elevated R_s. Use of conventional tabber and stringers for interconnecting the solar cells could further minimize any losses resulting from the manually effected interconnection of the solar cells [13,19,22].

The IV details of the module at different durations during the DHT are provided in appendix table A1. During the DHT, no degradation in the V_{oc} was observed in any of the modules. The V_{oc} of all the modules

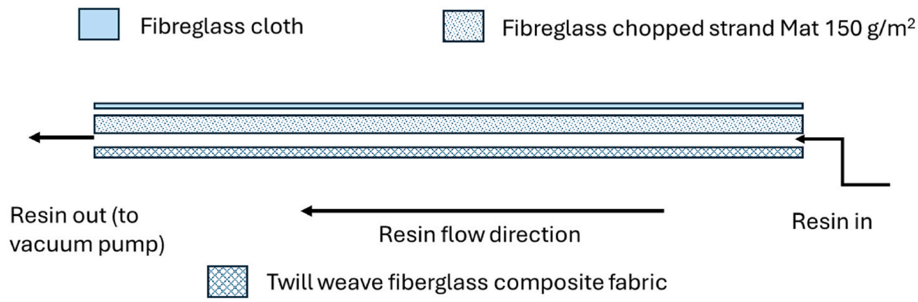

Fig. 9. Cross section schematic of the GRCF stack used for transmittance characterization using UV–VIS. It is similar to the final module prepared without the solar cells. The fibreglass cloth and the twill weave composite fabric were changed according to the scheme presented in Table 2.

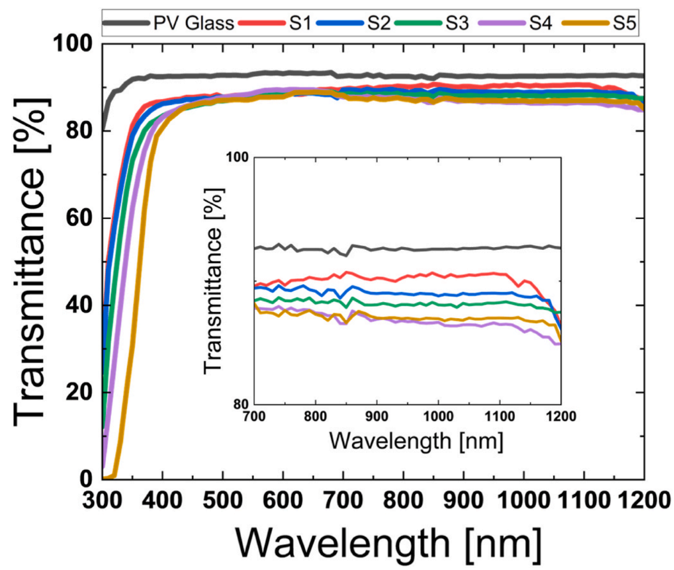

Fig. 10. Transmittance of the different GRCF stacks prepared according to the details given in Table 2.

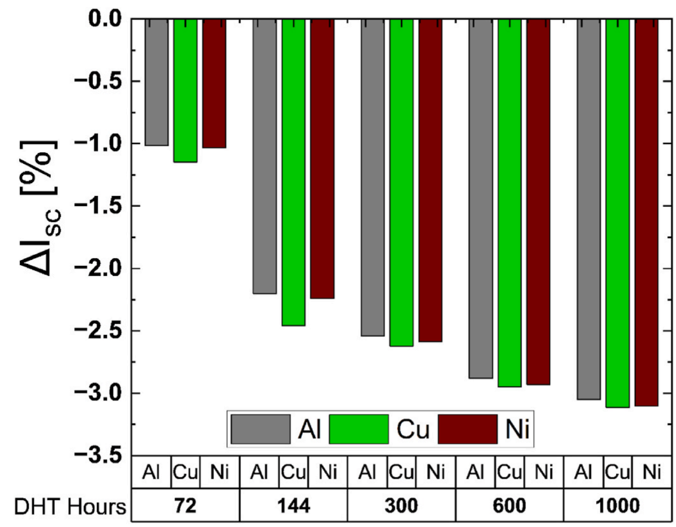

Fig. 11. ΔI_{sc} of the modules at different intervals (hours) during the damp heat test expressed as a percentage relative to the I_{sc} before the damp heat test.

Table 3
I-V characteristics of the fabricated modules before the damp heat test. The modules are designated by the material of the end strips. For each type of metal strip there were three modules, and each module was measured three times. For comparison, the solar cell characteristics as provided by the supplier are also mentioned.

	V_{oc} [V]	I_{sc} [A]	FF [%]	P_{max} [W]	R_s [Ω]	R_{sh} [Ω]
Al	1.4 ± 0.1	5.8 ± 0.1	69.4 ± 0.4	5.9 ± 0.1	0.04 ± 0.01	46.4 ± 1.6
Cu	1.4 ± 0.1	6.1 ± 0.2	70.5 ± 1.2	6.1 ± 0.1	0.03 ± 0.01	48.6 ± 2.1
Ni	1.4 ± 0.2	5.8 ± 0.3	61.9 ± 2.2	5.1 ± 0.2	0.06 ± 0.02	40.3 ± 3.1
Solar Cell (single)	0.715	5.8	81.4	3.4	NA	NA

after 1000 h of DHT was measured to be 1.4 ± 0.1V, which is similar to the V_{oc} of the modules before the DHT. Hence it can be surmised that no moisture ingress occurred in the modules and there was no loss in the passivation of the solar cells surface. Therefore, any changes in the performance of the modules can be attributed to the changes in I_{sc} and FF of the modules.

Fig. 11 shows the relative change in the I_{sc} (ΔI_{sc}) of the modules as a percentage of the original I_{sc} as the damp heat test progressed. This was calculated according to the formula,

$$\Delta I_{sc(m,t)} = \frac{I_{sc(m,t)} - I_{sc(m,0)}}{I_{sc(m,0)}} \times 100 \quad \text{(Eq-1)}$$

As seen from the figure, all modules exhibited similar degradation in the I_{sc} at different durations during the damp heat test. The average reduction (relative) in I_{sc} for all the modules taken together was 1.05 %, 2.3 % and 2.5 % for 72 h, 144 h and 300 h respectively. The average loss in I_{sc} was observed to be ∼ 3 % for all the modules at the end of 1000 h of damp heat test. The losses in all the modules are similar, which points towards the degradation in the GRCF layers during the damp heat test as all the modules are prepared with the similar structure and resin formulation. Since all the modules were prepared within a month, changes in ambient temperatures and the resin shelf life are expected to be minimum. The Isc of the module was found almost equal to the Isc value of the solar cells provided by the manufacturer. The exact reason behind this observation is no clear, however, the reduction in I_{sc} cannot be directly estimated from the transmittance of the optical stack test samples (Fig. 10). While determining the optical characteristics of the stack, the entire stack (including the front and the rear layers, Fig. 9) was used. Hence the transmittance of the stacks shown in Fig. 10 includes the absorption in the front layers, resin and the rear layer. However, only the top two layers and the resin contribute to the light absorption when the solar cell in encapsulated. Hence, we surmise that the absorption of the top two layers (including the resin) is significantly less than that of the entire stack. This is possible because the twill weave GRCF layer used at the rear is the densest (250 g/m^2) and causes the partial opacity observed at the edges of the mini-modules prepared (Fig. 8).

To further investigate the decrease in the I_{sc}, the GRCF stack (S2) used earlier for optical characterization was also subjected to damp heat test and the transmittance was measured. Fig. 12 shows the transmittance of the S2 GRCF stack (used for making the modules) at different intervals of the damp heat test. An enlarged part of the plot is also included in the inset to highlight the differences in the transmittance between 400 nm and 650 nm. The differences in the optical behaviour of the stack after 72 h and 144 h of the exposure is clearly visible, especially in the range of 300–700 nm. This corresponds to the observed reduction in the I_{sc} of the mini-modules. The relative reduction in the I_{sc} is largest after 72 and 144 h of damp heat test, after which there is a slower relative degradation in the I_{sc} of the mini-modules. Correspondingly, the transmittance of the GRCF stacks is almost similar after 300, 600 and 1000 h of damp heat test, though minute degradation in transmittance can be observed in the enlarged image. However, since the stacks include all the layers, it is not possible to resolve the loss in transmittance relative to the different GRCF layers in the stacks. Nevertheless, since the loss in I_{sc} of the module could mostly be attributed to the changes in the layers on top of the solar cells, the changes in the transmittance could be attributed to changes in the optical behaviour of the top layers and the resin. More detailed experiments with dedicated samples would be required to determine the contribution of each layer to the losses in I_{sc}, which left for a future work.

The degradation in the Isc has been linked to the changes in the chromatic behaviour of the layers on exposure to UV, high temperatures and moisture [18,19]. While no UV exposure tests were done in this work, changes in the chromatic response of the layers could be denied. Further, researchers have earlier attributed poor performance of such modules on poor optical coupling, air bubbles and cracks in the modules [13]. However, in this work, air bubbles or delamination were not observed after the damp heat test. Since visible signs of moisture ingress could not be observed in the panels, the reduced I_{sc} could be attributed to the change in the chromatic behaviour and visual response of the GRCF constituting the front layer of the modules.

Figs. 13 and 14 show the relative change in the FF (ΔFF) and maximum power output (ΔP_{max}) of the modules at various stages during the damp heat test respectively. The values were derived using the formula similar to eq-1. Since no degradation was observed in V_{oc} of the modules, the changes in the P_{max} can be attributed to the changes in I_{sc} and FF. The FF decreased by ~ 2 % immediately after the 72 h DHT, however, it did not deteriorate much further. At the end of 1000 h, the maximum deterioration in the FF was observed to be ~ 2.5 % in modules with Al end strips. The FF deterioration in the modules with the copper strips was always less than that in modules with Al strips, but more than that in the modules with the Ni strips. The differences in the relative degradation in FF for the modules with Cu strips exhibited some interesting characteristics. Initially, the relative degradation in the modules with Cu strips was similar to that in the modules with Ni strips; both of them being lower than the relative degradation of FF in the modules with Al strips. However, as the DHT progressed, the relative degradation in FF in the modules with Cu strips approached the value exhibited by the modules with Al strips; both of them being larger than the relative degradation in the modules with Ni strips. This could be interpreted as the change in electrical properties of the strips on exposure to moisture. While the moisture influences the Al strips early, the Cu and Ni strips are affected at a slower rate. Furthermore, the effect of moisture on the Cu strips progresses slowly but steadily over a longer duration than either Al or Ni strips. From the beginning until the end of the DHT, the modules with Cu strips exhibited the highest absolute FF (Table A1) and appeared be fairly corrosion resistant. However, detailed corrosion experiments would be needed to understand the impact of moisture on these metal strips, which is beyond the scope of this work and is left for future

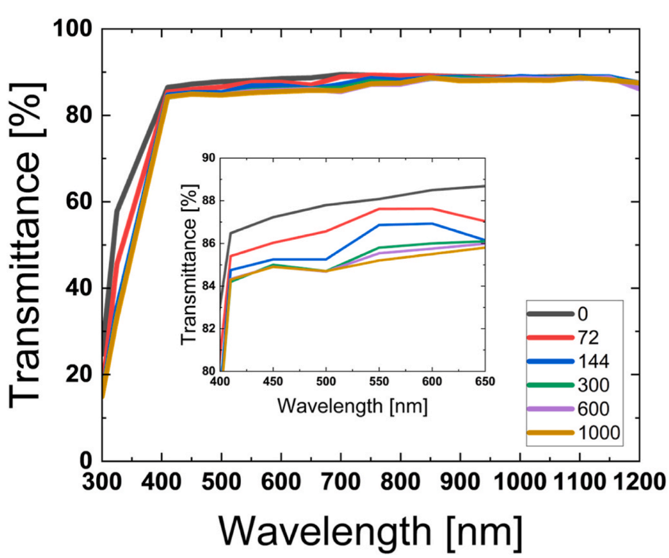

Fig. 12. Transmittance of the S2 GRCF stack used in the mini modules at different durations during the damp heat test. The hours of exposure after which the characterization has been done is mentioned in the legend.

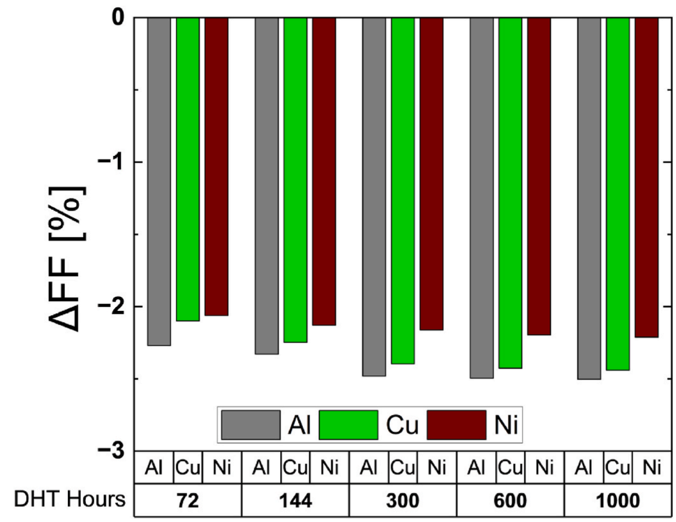

Fig. 13. ΔP_{max} of the modules after the damp heat test expressed as a percentage relative to the P_{max} before the damp heat test.

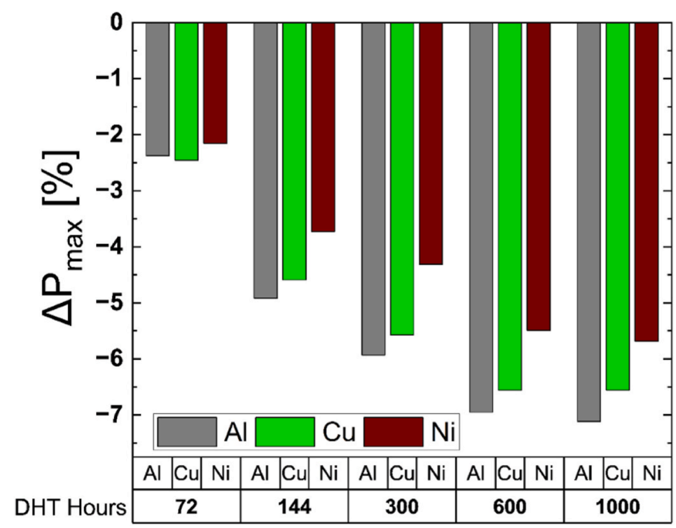

Fig. 14. ΔP_{max} of the modules after the damp heat test expressed as a percentage relative to the P_{max} before the damp heat test.

investigations. Throughout the test, the module with Al end strips registered the largest decrease in FF while the modules with Ni alloy end strips exhibited the lowest percent decrease in the FF. However, it should be noted, that the modules with Ni end strips had the lowest FF to begin with. Hence, it was observed that ΔP_{max} followed trend similar to ΔI_{sc}. The impact of the FF can be clearly seen on the ΔP_{max}. While both ΔP_{max} and ΔI_{sc} increased with increased duration of the damp heat test, the trend in the individual module types was not similar. While all the different modules had shown similar degradation in the ΔI_{sc}, the relative ΔP_{max} was largest for the modules fabricated with Al end strips and was least for the modules with Ni end strips due to the slight difference in the FF values.

Despite the difference in the relative change in power output, modules with Al and Cu end strips still exhibited ≈1 W power more than those with the Ni end strips after the 1000 h of damp heat test. After 1000 h of damp heat test, modules with Al end strips had lost ≈7.1 % of their initial power output, while those with nickel end strips had lost ≈5.7 % of their initial power output. The decrease in power matches with the corresponding reduction in the I_{sc} and FF.

Despite exhibiting lowest degradation in P_{max} and R_s, the resistance of the Ni alloy was substantially higher and the modules with end strips made from Ni alloy resulted in lowest power output. The cross-section area of the Al and Cu strips were similar (≈1 mm^2), the cross-section area of the Ni alloy was less than half of that (≈0.4 mm^2). Additionally, the resistivity of the Ni metal strip was two times that of Al and three times that of Cu strips. This could be the reason for the poor electrical performance of the modules with the Ni metal strips. The cross-sectional area of the metal strips can be changed to compensate for the lower resistivity of the metal strips. Since, the Ni metal strip has higher resistivity, the cross-sectional area should be larger to reduce the resistance of the strip for a given length.

3.3. Characterization of the modules using EL

EL of the modules was taken before the damp heat test and at regular intervals when the modules were retrieved for IV characterization. The EL images of the modules which survived the test did not reveal much information, as the changes in the EL were not visually discernible. However, defects and imperfections were easily visible using EL in some additional modules which failed the DH tests. For, example, some of the modules prepared with Al alloy cracked. EL images at different durations after the damp heat test for one such module are shown in Fig. 15. It could be clearly seen that the crack originated at the interconnection between the solar cells and at the end strips. While the exact reason for this could not be ascertained, this could be due to the release of the residual stresses which accumulated during the soldering process.

Further, while the glass fibres were not visible to naked eye after the module fabrication, they could be seen in the EL images of some of the modules, albeit with varying intensities. Furthermore, the longer the duration of the damp heat test, the easier it was to see the fibres in the EL images of such modules. Fig. 16 shows two EL images of the modules (not included in the study reported earlier), after DH 300 and after DH 1000, where the glass fibres were clearly visible throughout the surface of the modules. Since they were visible only on some of the modules, we hypothesize insufficient drying of the fibres prior to module fabrication as the reason behind this anomaly. These modules also did not perform well and shown huge deterioration after the DH test. In some cases, the P_{max} dropped by as much as 70 % after DH 1000. This could be the due to the residual moisture in the glass fibres [21,22], which could arise from the lack of process control in terms of the moisture content of the GRFP layers used for fabricating the modules. These could also result due to moisture ingress and absorption of moisture by the glass fibres due to improper lamination. However, further investigations would be required for a conclusive assessment of the reasons behind the appearance of glass fibres in the EL of only some of the modules and would be subject of further research.

4. Weight and costs considerations of the prepared GRCF modules

The completed module varied in thickness from 1.55 to 1.75 mm. The modules made with Al strips were slightly thicker as the Al strips were the thickest (Table 2). The modules ranged in weight from 87 to 95 g. The modules with Al metal strips weighed between 87 and 89 g while those with Ni and Cu end strips weighed between 92 and 95 g, with modules with copper strips were slightly heavier than those with nickel strips. The area of the prepared mini modules along with the extra polymer layer at the edges, was 275 x130 mm^2. This area was kept similar for all the modules. Therefore, the area specific weight (ASW) of the module was calculated to be 2.5 ± 0.1 kg/m^2. The ASW of the mini modules prepared in this work was estimated to be lower than the ASW of a typical full size glass-backsheet modules by a factor of ≈4 [13], and lower than the ASW of the commercial flexible panels by a factor of ≈2.

The power specific weight (PSW) of the modules (g/W) were calculated using the module weight and as fabricated P_{max}. The PSW of the modules (g/W) with Al, Cu and Ni strips were calculated as 14.7 ± 0.1, 15 ± 0.1 and 17.9 ± 0.3 g/W respectively. The PSW of a typical commercial glass-glass modules using IBC solar cells retailing online is 54.5 g/w (450 W, 24.5 kg) while that of the commercially available flexible modules is 27.3 g/W (330W, 9 kg, 1.623 m^2) [23]. Hence, despite the imperfections in the module fabrication process, the power specific weight was found to be lower than the commercial modules. Maintaining the V_{oc} and J_{sc} as reported earlier in Table 3 and if the FF is improved to 78 % for modules with Cu or Al end strips or to 75 % for the modules with Ni end strips, the PSW could be reduced to 13.8 g/W (for Al end strips) to 15.1 g/W (Ni end strips). This could be achieved by minimising the resistive losses which would be the aim of future research.

The approximate cost of the module was calculated to be in the range of 0.6–0.8 US$/watt. This is only slightly higher than the cost of IBC modules available commercially. However, this includes only the cost of the consumables such as the solar cells, GRCF layers, resins, metal end-strips, solder alloy and other consumables used in the fabrication of each mini module containing two solar cells. The 5 inch- IBC solar cells contributed ≈75 % to the total cost. The cost of the systems such as the pumps, electricity, worktable etc. are not included in these calculations.

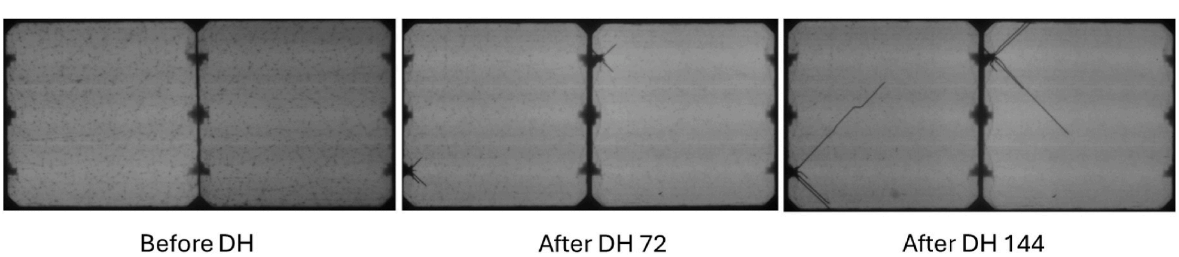

Fig. 15. EL images showing a module with Al connecting strips developing cracks after 72 h of damp heat test (DH72), The cracks further propagated after 144 h of damp heat test (DH 144). Such modules were replaced and were not included in the final analysis.

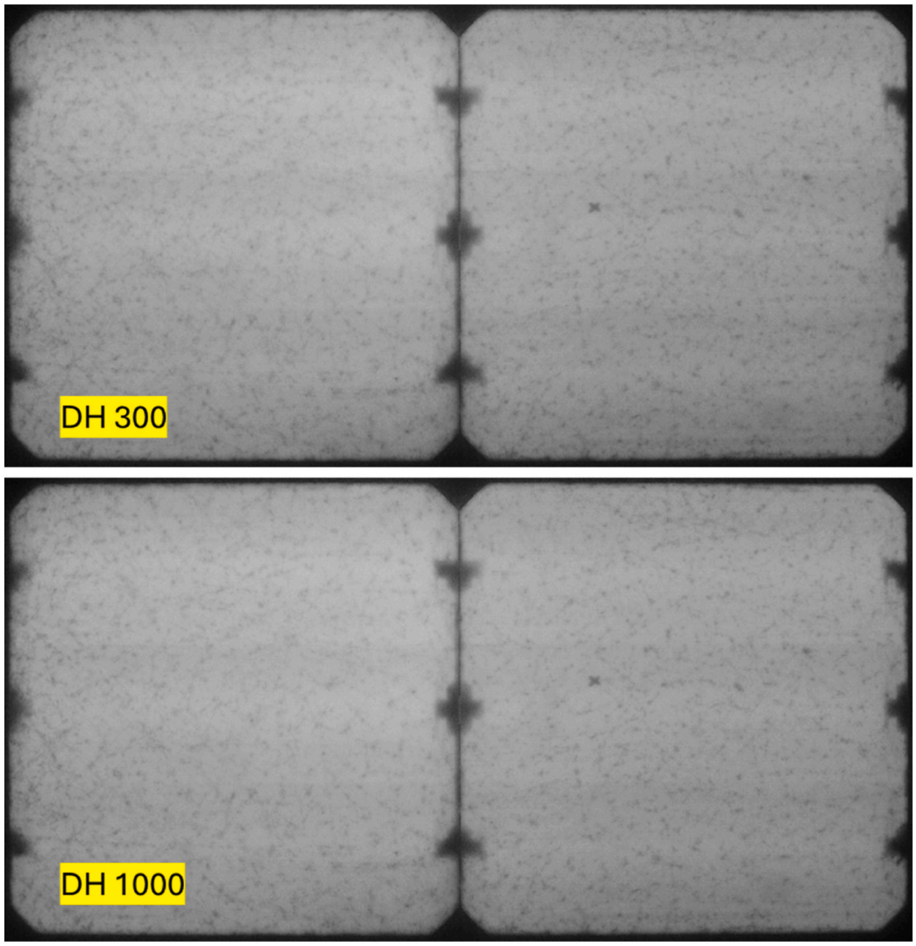

Fig. 16. EL images of two modules after DH 300 and DH 1000 where the individual glass fibres are clearly visible. For this module the drop in I_{sc} and consequently the maximum power was much higher.

The cost calculated from the materials costs incurred for fabricating the test modules, could be lower for large scale production. For example, we purchased only small number of solar cells and few metres of the glass fibre reinforced fabrics. Another important parameter could be the time taken to prepare such modules, which will decide the throughput for large scale commercial production of such modules. Further research efforts should also aim at improving the speed of the module fabrication process.

Mechanical properties of the modules prepared for this work using standard tests could not be evaluated. The modules are flexible and could be bent easily by hands (Fig. 17). However, the mechanical rigidity and the self-supportive nature of the modules can only be evaluated after preparing a full-size module (1.2–1.6 m^2). Nevertheless, module flexibility does not appear to be a limiting factor for vehicle applications as the surfaces meant for integration are almost flat or having extremely slight curvature (Fig. 1). Further mechanical tests should also evaluate the resistance of the modules to hail impact and vibrations, both of which are necessary for successful integration of the PV module with the vehicle.

5. Conclusion

In this work, IBC solar cells were used to fabricate two-cell mini-module using vacuum infusion process. The process was developed

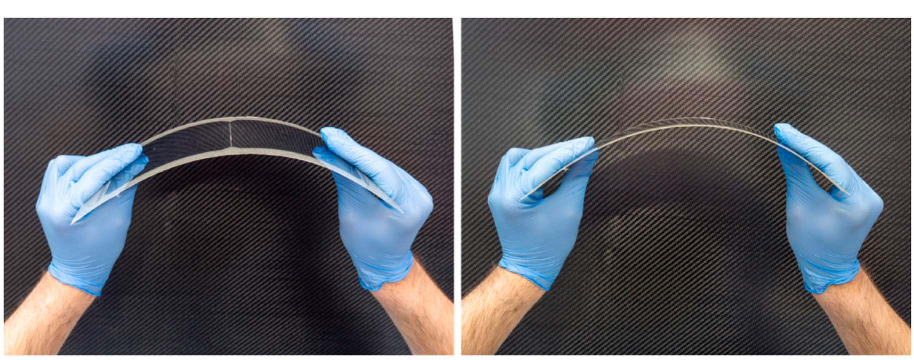

Fig. 17. The mini-modules were tested for flexibility by bending them with hands. Standard tests for the module flexibility will be carried out on the large-scale modules on a custom designed test-bench.

independently in out lab and was carried out in a non-controlled room open to atmosphere. This proof-of-concept work shows the possibility of fabrication of lightweight modules based on GRCF layers for applications in VIPV, without the use of laminator. The modules were designed to be bifacial. While bifaciality is not crucial for VIPV applications, these flexible modules could be used for other applications. An example of such an application were shown in artistically rendered images in Fig. 2. Design and development of the various components used for fabricating the module was discussed. It was observed that a compromise between transmissivity and mechanical strength is required for the design of such modules. The solar cells were interconnected manually using lead free solder paste, and three different metal alloys strips (Al, Cu and Ni based alloys) obtained from our industry partner were used as end strips. The modules were subjected to damp heat test and were characterized using IV and El measurements. Maximum 7 % relative power loss was recorded after DH 1000 in the modules with Al end strips. The power loss arose partially due to the loss in I_{sc} and due to increased R_s. The modules fabricated with Ni alloy suffered the largest loss in P_{max} in terms of magnitude due to the higher resistance of the Ni metal strips. Nevertheless, relative degradation in these modules was found to be the lowest. Analysis of the experimental data from this study shows that Cu strips (modified Cu alloy) are most suitable for fabricating the modules as they exhibited the highest FF and P_{max} values and were fairly stable in wet environment showing minimal degradation. While Ni alloys show the least degradation, they have huge resistance which limits the FF and the extractable power from these modules. Further improvement in electrical conductivity and corrosion resistance of Al alloys could make them an extremely attractive alternative to Cu strips. Some modules with Al end strips also developed cracks. Interestingly, such cracks were not observed in modules fabricated with Cu or Ni end strips. In some modules, while the glass fibres were not easily visible to naked eye, they were easily visible in the EL. Such modules were also significantly degraded after the damp heat tests, losing as much as 70 % of the initial power. This could be due to either residual moisture in the glass fibres or due to moisture ingress in the module during damp heat test. Further investigations into the causes behind the failure of these modules would help in developing lightweight weather resistant modules for applications in VIPV.

CRediT authorship contribution statement

Bartlomiej Fligier: Writing – original draft, Visualization, Resources, Project administration, Methodology, Investigation, Data curation. **Srinath Nalluri:** Validation, Resources, Methodology, Investigation, Data curation. **Bernard Moćko:** Validation, Methodology, Investigation. **Kazimierz Drabczyk:** Resources, Methodology, Investigation. **Grażyna Kulesza-Matlak:** Resources, Methodology, Investigation. **Katarzyna Jajczak:** Writing – original draft, Investigation, Funding acquisition. **Pradeep Padhamnath:** Writing – review & editing, Writing – original draft, Validation, Supervision, Resources, Methodology, Investigation, Funding acquisition, Formal analysis, Conceptualization.

Declaration of competing interest

The authors declare that they have no known competing financial interests or personal relationships that could have appeared to influence the work reported in this paper.

Acknowledgements

This research was funded by AGH University of Krakow, under the IDUB grant no 8854. This research is a part of AGH EKO-Energia which is a student research group at AGH comprising only undergraduate engineering students.

A part of the research is supported by the project No. 2022/45/P/ST5/02712 co-funded by the National Science Centre, Poland, and the European Union Framework Programme for Research and Innovation Horizon 2020 under the Marie Skłodowska-Curie grant agreement no. 945339.

A part of this research performed at the Solar Energy Research Institute of Singapore (SERIS) at the National University of Singapore. SERIS is supported by the National University of Singapore, the National Research Foundation (NRF), the Energy Market Authority of Singapore (EMA) and the Singapore Economic Development Board (EDB).

The authors would like to thank the industry partners who provided the advanced metal end strips for incorporating into the PV modules.

Appendix

Table A1
Measured IV data of the mini-modules at different hours during the damp heat test. The data represents the values of three modules for each metal strip and each module was measured three times (9 measurements for each data point)

DHT hours	Metal strip	V_{oc} [V]	I_{sc} [A]	FF [%]	P_{max}[W]
72	Al	1.4 ± 0.1	5.84 ± 0.06	67.86 ± 0.4	5.55 ± 0.4
	Cu	1.4 ± 0.1	6.03 ± 0.05	69.05 ± 0.2	5.83 ± 0.3
	Ni	1.4 ± 0.1	5.74 ± 0.05	60.65 ± 0.2	4.87 ± 0.4
144	Al	1.4 ± 0.1	5.77 ± 0.04	67.82 ± 0.2	5.48 ± 0.3
	Cu	1.4 ± 0.1	5.95 ± 0.04	68.95 ± 0.2	5.74 ± 0.3
	Ni	1.4 ± 0.1	5.67 ± 0.04	60.61 ± 0.3	4.81 ± 0.3
300	Al	1.4 ± 0.1	5.75 ± 0.02	67.72 ± 0.1	5.45 ± 0.2
	Cu	1.4 ± 0.1	5.94 ± 0.01	68.85 ± 0.2	5.73 ± 0.2
	Ni	1.4 ± 0.1	5.65 ± 0.02	60.59 ± 0.2	4.79 ± 0.2
600	Al	1.4 ± 0.1	5.73 ± 0.01	67.71 ± 0.1	5.43 ± 0.1
	Cu	1.4 ± 0.1	5.92 ± 0.01	68.83 ± 0.1	5.70 ± 0.1
	Ni	1.4 ± 0.1	5.63 ± 0.01	60.57 ± 0.1	4.77 ± 0.1
1000	Al	1.4 ± 0.1	5.72 ± 0.01	67.71 ± 0.1	5.42 ± 0.1
	Cu	1.4 ± 0.1	5.91 ± 0.01	68.82 ± 0.1	5.69 ± 0.1
	Ni	1.4 ± 0.1	5.62 ± 0.01	60.56 ± 0.1	4.76 ± 0.1

Data availability

No data was used for the research described in the article.

References

[1] E. Karden, P. Shinn, P. Bostock, J. Cunningham, E. Schoultz, D. Kok, Requirements for future automotive batteries–a snapshot, J. Power Sources 144 (2005) 505–512.

[2] M. Anderman, The challenge to fulfill electrical power requirements of advanced vehicles, J. Power Sources 127 (2004) 2–7.

[3] G. Almonacid, F.J. Muñoz, J. De La Casa, J.D. Aguilar, Integration of PV systems on health emergency vehicles. The FIVE project, Prog. Photovoltaics Res. Appl. 12 (2004) 609–621.

[4] M. Geca, M. Wendeker, L. Grabowski, A city bus electrification supported by the photovoltaic power modules, SAE Techn. Pap. (2014).

[5] U. Eitner, M. Ebert, T. Zech, C. Schmid, A. Watts, M. Heinrich, Solar potential on commercial trucks: results of an irradiance measurement campaign on 6 trucks in Europe and USA, in: European Photovoltaic Solar Energy Conference and Exhibition, EU PVSEC, 2017, 2017.

[6] M. Kühnel, B. Hanke, S. Geißendörfer, K. von Maydell, C. Agert, Energy forecast for mobile photovoltaic systems with focus on trucks for cooling applications, Prog. Photovoltaics Res. Appl. 25 (2017) 525–532.

[7] M. Heinrich, C. Kutter, F. Basler, M. Mittag, L.E. Alanis, D. Eberlein, A. Schmid, C. Reise, T. Kroyer, D.H. Neuhaus, Potential and challenges of vehicle integrated photovoltaics for passenger cars, in: Present. 37th Eur. PV Sol. Energy Conf. Exhib, 2020, p. 4229.

[8] C. Kutter, L.E. Alanis, D.H. Neuhaus, M. Heinrich, Yield potential of vehicle integrated photovoltaics on commercial trucks and vans, in: Presented at the 38th European PV Solar Energy Conference and Exhibition, 2021, p. 10.

[9] M.C. Brito, T. Santos, F. Moura, D. Pera, J. Rocha, Urban solar potential for vehicle integrated photovoltaics, Transp. Res. D Transp. Environ. 94 (2021) 102810.

[10] J. Govaerts, B. Luo, T. Borgers, R. Van Dyck, A. van der Heide, L. Tous, A. Morlier, F. Lisco, L. Cerasti, M. Galiazzo, Development and testing of light-weight PV modules based on glass-fibre reinforcement, EPJ Photovoltaics 13 (2022) 13.

[11] B. Luo, J. Govaerts, R. Van Dyck, T. Borgers, B. Ruttens, M.C. Paesa, J. D'Haen, L. Tous, H.S. Radhakrishnan, M. Daenen, Development and thermo-mechanical reliability assessment of fiber reinforced polymers in lightweight PV modules towards vehicle-integrated photovoltaics, Sol. Energy Mater. Sol. Cell. 259 (2023) 112455.

[12] J. Govaerts, B. Luo, T. Borgers, R. Van Dyck, A. van der Heide, L. Tous, A. Morlier, F. Lisco, L. Cerasti, M. Galiazzo, Development and testing of light-weight PV modules based on glass-fibre reinforcement, EPJ Photovoltaics 13 (2022) 13.

[13] M.A. Schüler, M.-D. Goth, J. Markert, L.E. Alanis, C. Kutter, F. Basler, M. Heinrich, D.H. Neuhaus, Towards fiber-reinforced front-sheets for lightweight PV modules in VIPV, Sol. Energy Mater. Sol. Cell. 277 (2024) 113048.

[14] A.H.M.E. Reinders, H. De Wit, A. de Boer, Design of fibre reinforced PV concepts for building integrated applications, in: 24th European Photovoltaic Solar Energy Conference and Exhibition, EU PVSEC 2009, WIP-Renewable Energies, 2009, pp. 3940–3944.

[15] C. Pascual, J. De Castro, A. Schueler, T. Keller, Integration of dye solar cells in load-bearing translucent glass fiber-reinforced polymer laminates, J. Compos. Mater. 51 (2017) 939–953.

[16] A.S. Budiman, R. Sahay, K. Agarwal, R. Fajarna, F.E. Gunawan, A. Baji, N. Raghavan, Modeling impact mechanics of 3D helicoidally architected polymer composites enabled by additive manufacturing for lightweight silicon photovoltaics technology, Polymers 14 (2022) 1228.

[17] A.H.M.E. Reinders, H. De Wit, A. de Boer, Design of fibre reinforced PV concepts for building integrated applications, in: 24th European Photovoltaic Solar Energy Conference and Exhibition, EU PVSEC 2009, WIP-Renewable Energies, 2009, pp. 3940–3944.

[18] G. Imbuluzqueta, N. Yurrita, J. Aizpurua, F.J. Cano, O. Zubillaga, Composite material with enhanced ultraviolet performance stability for photovoltaic modules, Sol. Energy Mater. Sol. Cell. 200 (2019) 109947, https://doi.org/10.1016/j.solmat.2019.109947.

[19] N. Yurrita, J. Aizpurua, W. Cambarau, G. Imbuluzqueta, J.M. Hernández, F. J. Cano, O. Zubillaga, Photovoltaic modules encapsulated in composite material modified with ultraviolet additives, Sol. Energy Mater. Sol. Cell. 230 (2021) 111250, https://doi.org/10.1016/j.solmat.2021.111250.

[20] T. Gorter, A.H.M.E. Reinders, A comparison of 15 polymers for application in photovoltaic modules in PV-powered boats, Appl. Energy 92 (2012) 286–297.

[21] N. Yurrita, J. Aizpurua, W. Cambarau, G. Imbuluzqueta, J.M. Hernández, F. J. Cano, I. Huerta, E. Rico, T. del Caño, S. Wölper, F. Haacke, O. Zubillaga, Composite material incorporating protective coatings for photovoltaic cell encapsulation, Sol. Energy Mater. Sol. Cell. 245 (2022) 111879, https://doi.org/10.1016/j.solmat.2022.111879.

[22] F.J. Cano, G. Imbuluzqueta, N. Yurrita, J. Aizpurua, J.M. Hernández, W. Cambarau, O. Zubillaga, Composite material with enhanced recyclability as encapsulant for photovoltaic modules, Heliyon 9 (2023) e20048, https://doi.org/10.1016/j.heliyon.2023.e20048.

[23] sunpoweredyachts.com, Maxeon® Air 330W flex, (n.d.). https://www.sunpoweredyachts.com/product-page/maxeon-air-330w-flex?srsltid=AfmBOopuRF_geT1-U9dDPzEV1Ukq9in4VUb84WXsRLQUTegegXkU9o3A (accessed May 13, 2025).